Available online at www.sciencedirect.com
ScienceDirect
Journal of Hazardous Materials 152 (2008) 1229–1236
Journal of Hazardous Materials
www.elsevier.com/locate/jhazmat

Preparation and enhanced daylight-induced photocatalytic activity of C,N,S-tridoped titanium dioxide powders

Minghua Zhou [a,b], Jiaguo Yu [b,*]

[a] *Staff Room of Chemistry, Yunyang Medical College, Shiyan 442000, Hubei, PR China*
[b] *State Key Laboratory of Advanced Technology for Material Synthesis and Processing, Wuhan University of Technology, Luoshi Road 122, Wuhan 430070, PR China*

Received 23 April 2007; received in revised form 31 July 2007; accepted 31 July 2007
Available online 7 August 2007

Abstract

A simple method for preparing highly daylight-induced photoactive nanocrystalline C,N,S-tridoped TiO_2 powders was developed by a solid-phase reaction. The as-prepared TiO_2 powders were characterized by X-ray diffraction (XRD), X-ray photoelectron spectroscopy (XPS), UV–vis diffuse reflectance spectra, N_2 adsorption–desorption measurements and transmission electron microscopy (TEM). The photocatalytic activity was evaluated by the photocatalytic oxidation of formaldehyde under daylight irradiation in air. The results show that daylight-induced photocatalytic activities of the as-prepared TiO_2 powders were improved by C,N,S-tridoping. The C,N,S-tridoped TiO_2 powders exhibited stronger absorption in the near UV and visible-light region with red shift in the band-gap transition. When the molar ratio of $CS(NH_2)_2$ to xerogel TiO_2 powders (prepared by hydrolysis of $Ti(OC_4H_9)_4$ in distilled water) (R) was kept in 3, the daylight-induced photocatalytic activities of the as-prepared C,N,S-tridoped TiO_2 powders were about more than six times greater than that of Degussa P25 and un-doped TiO_2 powders. The high activities of the C,N,S-tridoped TiO_2 can be attributed to the results of the synergetic effects of strong absorption in the near UV and visible-light region, red shift in adsorption edge and two phase structures of un-doped TiO_2 and C,N,S-tridoped TiO_2.

Keywords: TiO_2; Daylight-induced; Photocatalytic activity; C,N,S-tridoping; Formaldehyde

1. Introduction

Daylight-driven semiconductor-mediated photocatalytic technology has attracted much attention because it is a vital step in using solar energy to eliminate undesired chemical substances for environment conservation and to split water for green-energy hydrogen production [1]. Among various semiconductors, TiO_2 has been proved to be the most suitable photocatalyst for widespread environmental applications because of its biological and chemical inertness, strong oxidizing power, non-toxicity and long-term stability against photo and chemical corrosion [2–11]. However, the anatase TiO_2 can be activated only under UV light of wavelengths <387 nm irradiation due to its large band-gap of 3.2 eV. Therefore, the optical response of TiO_2 shifting into the visible-light region will enhance its photocatalytic activity under daylight or solar irradiation due to the solar spectrum usually containing about 4% UV light [10,11]. Fortunately, recent study have revealed that the shortcomings of TiO_2 can be overcome by doping it with some non-metallic elements [11–21] such as N, F, S, C, B, etc. Especially, Asahi et al. reported that the photocatalytic activity and hydrophilicity of TiO_2 could be enhanced by nitrogen doped into the substitutional sites of TiO_2 ($TiO_{2-x}N_x$) [21]. Umebayashi et al. [22–24] have succeeded to synthesize S-doped TiO_2, which was used as an efficient visible-light-induced photocatalyst for photocatalytic degradation of methylene blue. Ohno et al. [25–27] found that S could be incorporated as cations and replaced Ti ions in the TiO_2 photocatalysts. Zhao et al. [28] and Majima and co-workers [29] reported that doping TiO_2 with boron or sulfur could also reduce its band-gap and shift its optical response to the visible-light region. Recently, we prepared daylight-induced N,S-codoped TiO_2 photocatalysts with a high-photocatalytic activity using $Ti(SO_4)_2$ and $NH_3{\cdot}H_2O$ as presursors [30]. Undeniably, the

* Corresponding author.
E-mail address: jiaguoyu@yahoo.com (J. Yu).

0304-3894/$ – see front matter © 2007 Elsevier B.V. All rights reserved.
doi:10.1016/j.jhazmat.2007.07.113

modification of TiO_2 photocatalysts involves the doping with non-metal elements resulting in a desired band-gap narrowing and an enhancement in the photocatalytic efficiency under daylight-induced. This technique opens up a new possibility for the development of solar- or daylight-induced photocatalytic materials. However, to the best of our knowledge, the effects of C,N,S-tridoping on the photocatalytic activity of TiO_2 powders have not been reported. This work may also provide new insights into the preparation of highly visible-light photoactive TiO_2 powders.

2. Experimental

2.1. Preparation

All chemicals used in this study were reagent-grade without further purification. The xerogel TiO_2 powders were synthesized by hydrolysis of $Ti(OC_4H_9)_4$ in a distilled water. The details are as follows: $Ti(OC_4H_9)_4$ (8.8 ml) was added dropwise into a 100 ml distilled water in a 250 ml beaker under continuous stirring for 120 min. After hydrolysis reaction, the white precipitate was centrifuged, and then washed with distilled water for five times. The obtained white gels were dried under vacuum at 80 °C for 10 h and were ground to obtain powdered samples. To prepare doped TiO_2 samples, the as-prepared white xerogel TiO_2 powders were mixed with thiourea and then calcined at 500 °C in air for 3 h. The molar ratio of thiourea to TiO_2 (R) is 0, 1, 2, 3 and 6, and the obtained powders were labeled as TiO_2-0, TiO_2-1, TiO_2-2, TiO_2-3 and TiO_2-6, respectively. The color of the calcined powder samples changes and is from white to pale yellow with increasing R.

2.2. Characterization

The X-ray diffraction (XRD) patterns obtained on a X-ray diffractometer (type HZG41B-PC) using Cu Kα irradiation at a scan rate of 0.05° $2\theta\,s^{-1}$ were used to determine the identity of any phase present and their crystallite size. The accelerating voltage and the applied current were 15 kV and 20 mA, respectively. The average crystallite sizes of TiO_2 were determined according to the Scherrer equation using the full-width half-maximum data of each phase after correcting the instrumental broadening. The Brunauer–Emmett–Teller (BET) surface area (S_{BET}) of the powders was analyzed by nitrogen adsorption in an ASAP2020 surface area and porosity analyzer (Micromeritics, USA). All the samples and Degussa P25 were degassed at 180°C prior to nitrogen adsorption measurements. The BET surface area was determined by a multipoint BET method using the adsorption data in the relative pressure (P/P_0) range of 0.05–0.25. Desorption isotherm was used to determine the pore size distribution via the Barret–Joyner–Halender (BJH) method with cylindrical pore size [31]. The nitrogen adsorption volume at the relative pressure (P/P_0) of 0.994 was used to determine the pore volume and average pore sizes. Crystallite sizes and shapes were observed using transmission electron microscopy (TEM) (JEOL 1200EX, Japan). X-ray photoelectron spectroscopy (XPS) measurements were done with a Kratos XSAM800 XPS system with Mg Kα source and a charge neutralizer; all the binding energies were referenced to the C 1s peak at 284.8 eV of the surface adventitious carbon. UV–vis diffused reflectance spectra of TiO_2 powders were obtained for the dry-pressed disk samples using a UV–vis spectrophotometer (UV2550, Shimadzu, Japan.). $BaSO_4$ was used as a reflectance standard in a UV–vis diffuse reflectance experiment.

2.3. Measurement of photocatalytic activity

The photocatalytic activity experiments of the prepared TiO_2 powders and Degussa P25 for the oxidation of formaldehyde in air were performed at ambient temperature using a 15 L photocatalytic reactor. The detailed experimental process can be found in our previous studies [32,33]. The weight of catalysts used for each experiment was kept 0.20 g and the initial concentration of formaldehyde after adsorption equilibrium was controlled at 200 ± 10 ppm. Integrated daylight intensity was 0.46 ± 0.01 mW/cm^2 with the peak intensity of 420 nm. Each set of experiment in daylight illumination was performed for 120 min.

The photocatalytic activity of the catalysts can be quantitatively evaluated by comparing the removal efficiency of reactant (RE (%)). RE (%) was calculated according to the following equation [32]:

$$\mathrm{RE}\,(\%) = \frac{[\mathrm{gas}]_0 - [\mathrm{gas}]_t}{[\mathrm{gas}]_0} \times 100 \qquad (1)$$

where $[\mathrm{gas}]_0$ and $[\mathrm{gas}]_t$ represent the initial equilibrium concentration and reaction concentration of reactant, respectively.

3. Results and discussion

3.1. Phase structures

XRD was used to investigate the phase structure of the as-prepared TiO_2 powders at 500 °C. Fig. 1 shows the effects of R on the phase structures of the TiO_2 powders. All diffraction

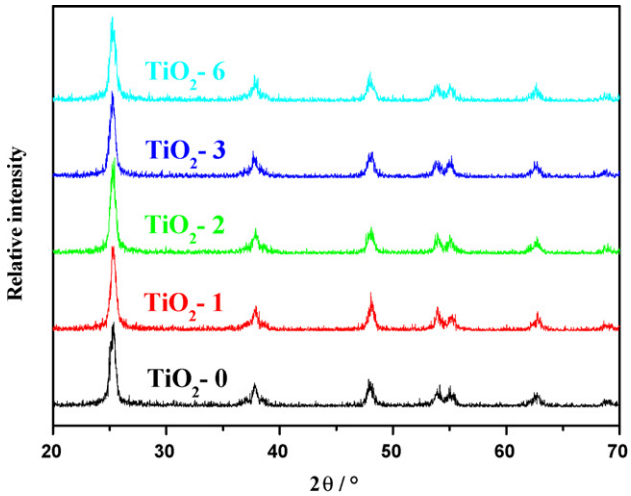

Fig. 1. XRD patterns of the un-doped and tri-doped TiO_2 powders calcined at 500 °C.

Table 1
Effects of R on physical properties of the un-doped and tri-doped TiO_2 powders

Sample	Phase content[a]	Crystalline size[b] (nm)	Surface area[c] (m^2/g)	Pore volume[d] (cm^3/g)	Average pore size (nm)
TiO_2-0	A	19.5	83.4	0.31	14.6
TiO_2-1	A	19.4	83.7	0.35	16.5
TiO_2-2	A	18.5	84.5	0.34	16.9
TiO_2-3	A	18.3	88.4	0.32	13.5
TiO_2-6	A	16.6	93.8	0.30	13.4
P25	A(80%) + R(20%)	30.0	45.0	0.06	3.8

[a] A and R denote anatase and rutile, respectively.
[b] Average crystalline size of TiO_2 was determined by XRD using Scherrer equation.
[c] The BET surface area was determined by a multipoint BET method using the adsorption data in P/P_0 range from 0.05 to 0.25.
[d] Pore volume and average pore size were determined by nitrogen adsorption volume at $P/P_0 = 0.994$.

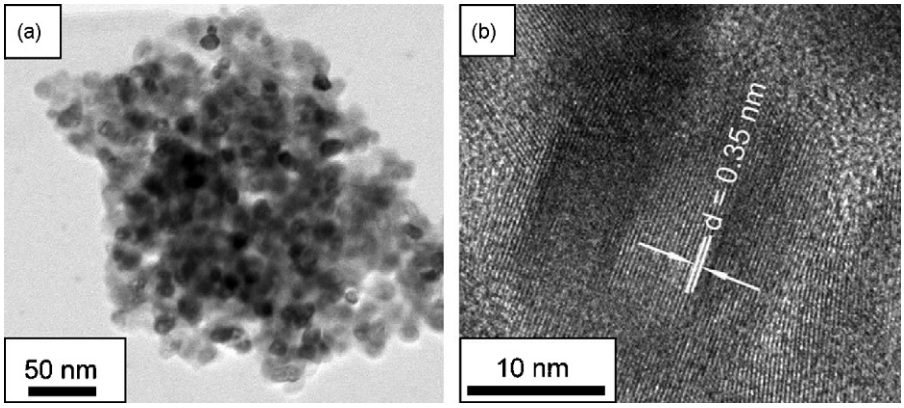

Fig. 2. TEM (a) and HRTEM (b) images of the tri-doped sample TiO_2-3.

peaks of the calcined powders were indexed to pure anatase phase of TiO_2 (JPCDS Card: 86-1157, space group: $I4_1/amd$). It can be seen that the R slightly influences the crystallization of the TiO_2 powders. With increasing R, the peak intensities of anatase slightly decrease and the width of the (1 0 1) plane diffraction peak of anatase ($2\theta = 25.4^\circ$) becomes broader. Therefore, it is reasonable to deduce that the larger R, the poorer the crystallization of the TiO_2 powders, and the smaller the crystallite size of TiO_2 (as shown in Table 1).

The microstructure of TiO_2 powders was further studied by TEM and HRTEM. Fig. 2(a) shows the TEM image of the TiO_2 powders prepared at $R = 3$. It can be observed from Fig. 2(a) that the nanocrystallite appears an agglomerated status, and mesoporous structures without a long-range order. The size of the primary particles estimated from the TEM image was about 17 ± 2 nm, which was in good agreement with the value (18.3 nm) calculated from XRD pattern using the Scherrer equation (as shown in Table 1). Fig. 2(b) shows the corresponding HRTEM image of the prepared sample TiO_2-3. It shows clear lattice fringes, which allowed for the identification of crystallographic spacing. The fringe spacing of ca. 0.35 nm matches that of the (1 0 1) crystallographic plane of TiO_2 anatase.

3.2. BET specific surface areas and pore structure

All the as-prepared TiO_2 powders have similar nitrogen adsorption–desorption isotherms and pore size distribution curves. Therefore, Fig. 3 only presents the nitrogen adsorption–desorption isotherm and pore size distribution (inset) of the C,N,S-tridoped sample TiO_2-3. It can be seen that isotherm of the sample TiO_2-3 was of types IV (BDDT classification) [31]. At high-relative pressure range from 0.6 to 1.0, the isotherm exhibits a hysteresis loop of type H2 associated with the ink bottle pores, indicating that the powders contain mesopores (2–50 nm). The corresponding pore size distribution curve of the tri-doped sample TiO_2-3 is also shown in Fig. 3 (inset). It can be seen that the tri-doped sample TiO_2-3 exhibits

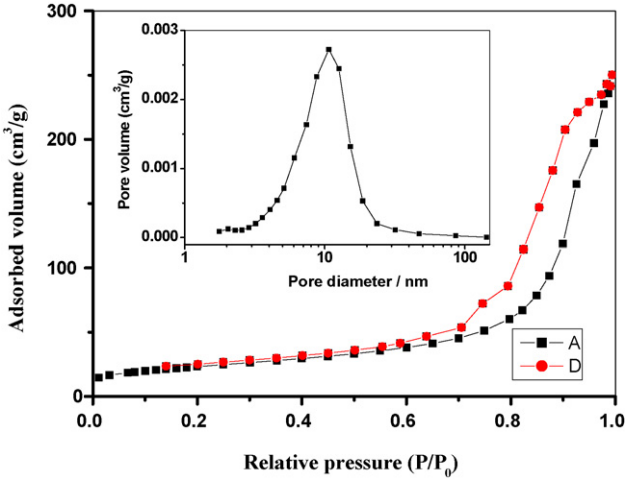

Fig. 3. N_2 adsorption–desorption isotherm and pore size distribution curve (inset) of the tri-doped sample TiO_2-3.

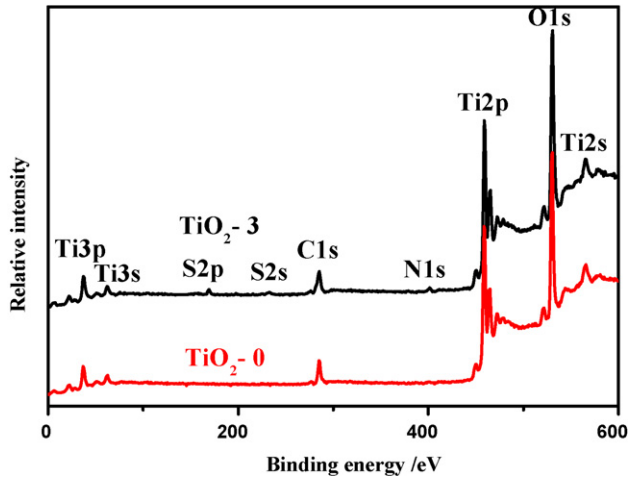

Fig. 4. XPS survey spectra of the un-doped sample TiO_2-0 and tri-doped sample TiO_2-3.

a wide pore size distribution (2–50 nm) with the average pore diameters about 13.5 nm.

Table 1 shows the effects of *R* on the physical properties of the TiO_2 powders. It can be seen that un-doped TiO_2 powder calcined at 500 °C shows a large specific surface area and pore volume, and their values reach 83.7 m^2/g and 0.31 cm^3/g, respectively. With increasing *R*, the specific surface areas increase slightly. This is due to the decrease in the crystallite sizes of the tri-doped TiO_2 powders.

3.3. XPS analysis

Fig. 4 shows the XPS survey spectra of the TiO_2-0 and TiO_2-3 powders. It can be seen that the un-doped sample TiO_2-0 only contains Ti, O and C elements, with sharp photoelectron peaks appearing at binding energies of 458 (Ti 2p), 531 (O 1s) and 285 eV (C 1s). The atomic ratio of Ti to O of the sample TiO_2-0 is about 2, in good agreement with the nominal atomic composition of TiO_2. The carbon peak is attributed to the residual carbon from the sample and adventitious hydrocarbon from XPS instrument itself. On the contrary, the doped sample TiO_2-3 not only contains Ti, O and C, but also a small amount of N and S atoms (binding energies at 401 and 169 eV, respectively), which probably come from the precursor $CS(NH_2)_2$ during the calcination.

Fig. 5(a) and (b) show the corresponding high-resolution XPS spectra of C 1s region of the samples TiO_2-0 and TiO_2-3, respectively. It can be seen that the C 1s region of the sample TiO_2-0 is only one symmetry peak and its binding energy at about 285.0 eV corresponds to carbons of saturated hydrocarbon groups ($–CH_3$, $–CH_2–$) [34], which come from the residual carbon in the sample or adventitious hydrocarbon from XPS instrument itself. However, the C 1s region of the sample TiO_2-3 can be deconvoluted into two peaks. The main peak at about 285.0 eV is ascribed to the saturated hydrocarbon groups mentioned above and a small peak at about 282.1 eV is ascribed to Ti–C bonds [35]. Of course, its formation mechanism is still needed to be further investigated.

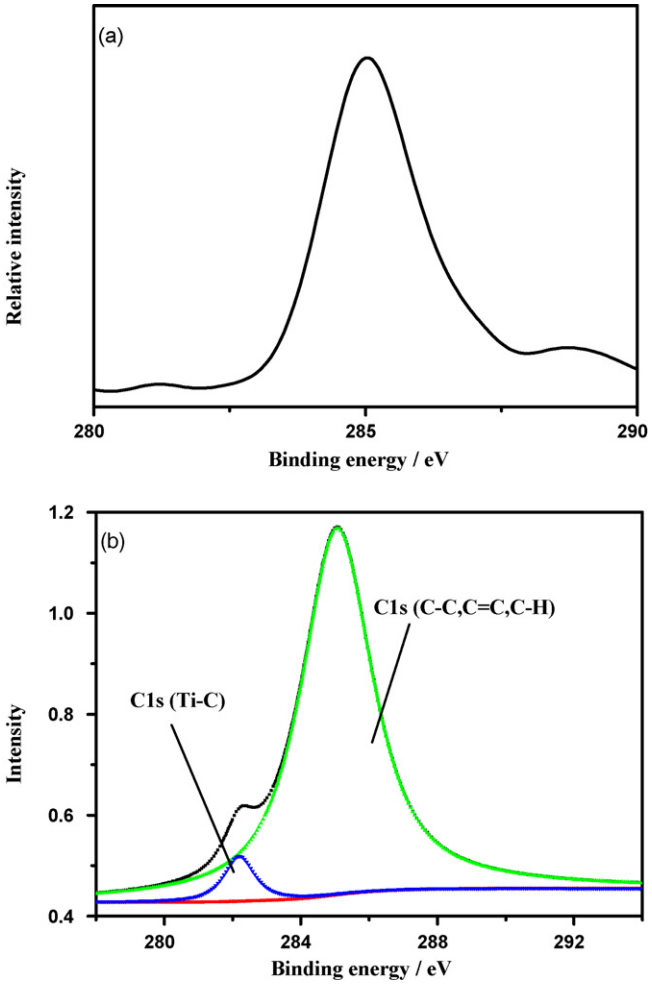

Fig. 5. High-resolution XPS spectra of C 1s region of the un-doped sample TiO_2-0 (a) and tri-doped sample TiO_2-3 (b).

Fig. 6 shows the corresponding high-resolution XPS spectra of the N 1s region taken from the sample TiO_2-3. It is interesting to note that the curve of the N 1s region of the sample TiO_2-3 can be deconvoluted into three peaks. A small one is

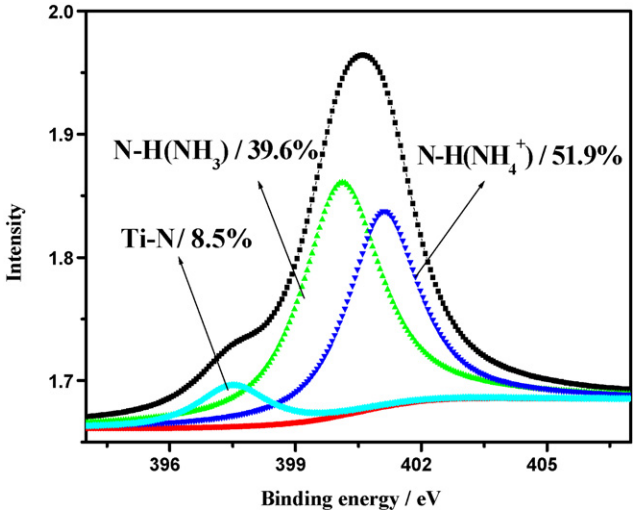

Fig. 6. High-resolution XPS spectra for the N 1s region of the sample TiO_2-3.

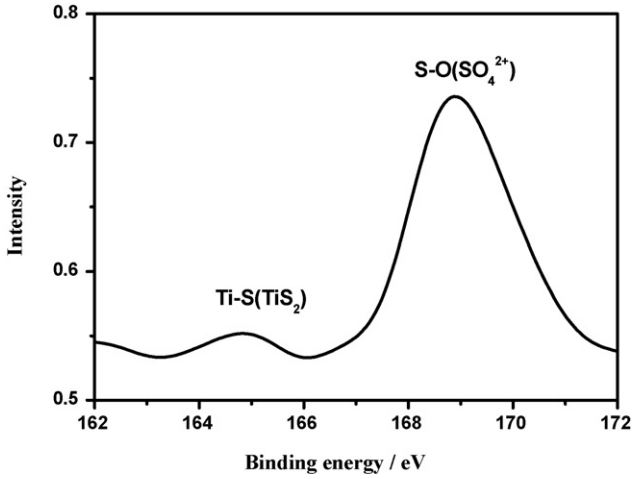

Fig. 7. High-resolution XPS spectrum of the S 2p region of the sample TiO_2-3.

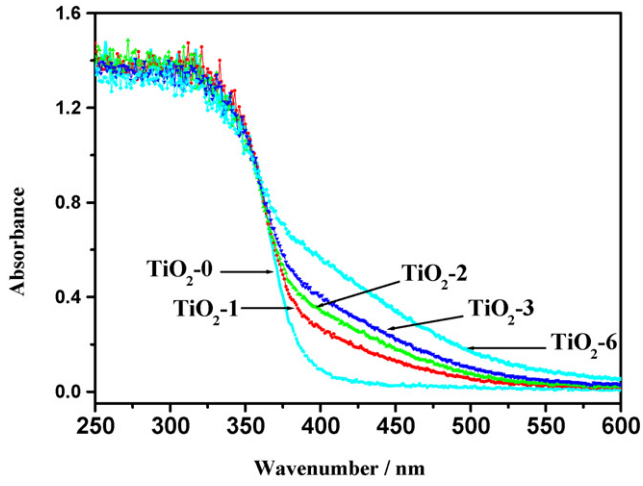

Fig. 8. UV–vis absorption spectra of the un-doped and tri-doped TiO_2 powders calcined at 500 °C.

attributed to the Ti–N (binding energy at 397.4 eV) [36–38], which is probably formed by a nucleophilic substitution reaction between $CS(NH_2)_2$ and TiO_2 during the calcination [11]. The other two peaks at about 400.0 and 401.1 eV are probably assigned to some NH_3 and NH_4^+ adsorbed on the surface of TiO_2, respectively [11,30].

Fig. 7 shows the high-resolution XPS spectrum of the S 2p region, taken on the surface of tri-doped sample TiO_2-3. It can be seen that the peak of S 2p contains two isolated peaks at binding energies of 169.0 and 164.8 eV, which can be attributed to the S(+VI) and S(−II), respectively. The S(+VI) may be assigned to the SO_4^{2-} ions adsorbed on the surface of TiO_2 powders. The peak at 164.8 eV corresponds to the Ti–S bond due to the fact that S atoms replace O atoms in the TiO_2 lattice [39]. It can be reasonable to deduce that if the S^{2-} ions replace the O^{2-} ions in the lattice of TiO_2, a lattice distort may be created due to different ionic radius between S^{2-} (1.7 Å) and O^{2-} (1.22 Å) [40]. XRD results further confirm the above deduction. The cell parameters a and c (calculated according to XRD result) of the tri-doped sample TiO_2-3 calcined at 500 °C were 3.787 and 9.514 Å, respectively, which were slightly bigger than those of pure anatase TiO_2 (JPCDS Card: 86-1157, $a = 3.783$ Å, $c = 9.497$ Å, space group: $I4_1/amd$) [30,41]. According to the above XPS results, no Ti–C, Ti–N and Ti–S peak was observed in the un-doped sample TiO_2-0, further implying that C, N and S elements were in situ doped into TiO_2 powders during calcination. The exact amounts of C, N and S in TiO_2 (TiO_2-3) were characterized by XPS and their atomic percentage are 2.6, 1.3 and 1.1%. Further XPS investigations show that the content of the C, N and S elements increases with increasing R in the prepared TiO_2 powders, while the ratio of C:N:S is not in agreement with that of C:N:S in the precursor $CS(NH_2)_2$.

3.4. UV–vis diffuse reflectance spectra

Usually, anions doping obviously influences light absorption characteristics of TiO_2 [19–21,28,29]. Fig. 8 shows the UV–vis absorption spectra of the C,N,S-tridoped TiO_2 powders. A significant increase in the absorption at wavelengths shorter than 400 nm can be assigned to the intrinsic band-gap absorption of TiO_2. The absorption spectra of the C,N,S-tridoped TiO_2 samples show a stronger absorption in the UV–vis light region and a red shift in the adsorption edge. Undoubtedly, these results reveal that the nonmetal elements are indeed incorporated into the lattice of TiO_2, thus altering its crystal and electronic structures [30].

The red shift is ascribed to the fact that C,N,S-tridoping can narrow the band-gap of the TiO_2 by mixing the orbit O 2p with C 2p, N 2p and S 3p orbits, respectively. Further observation shows that the absorbance increases with increasing R. Without doping, the absorbance of TiO_2 in the near UV and visible-light region is lower than that of other doped samples. When R reaches 6, the absorbance of C,N,S-tridoped TiO_2 is obviously higher than that of other doped sample in the near UV and visible-light region. This may be attributed to the fact that a high R can induce more C, N and S atoms doped into the lattice of TiO_2, resulting a large band-gap narrowing.

The absorption edge shifts to longer wavelengths for the C,N,S-tridoped TiO_2 powders with increasing R. This clearly indicates a decrease in the band-gap energy of TiO_2. The indirect band-gap energies of the C,N,S-tridoped TiO_2 powders can be estimated from a plot of $(\alpha h\nu)^{1/2}$ versus photo energy ($h\nu$). The intercept of the tangent to the plot will give a good approximation of the indirect band-gap energies of the samples. The relation between the absorption coefficient (α) and incident photon energy ($h\nu$) can be written as follow:

$$\alpha = \frac{B_i(h\nu - E_g)^2}{h\nu} \quad (2)$$

where B_i is absorption constants for indirect transitions [42–44]. The plots of $(\alpha h\nu)^{1/2}$ versus $h\nu$ are presented in Fig. 9. The indirect band-gap energies estimated from the intercept of the tangents to the plots are 3.2, 2.8, 2.5, 2.4 and 2.2 eV for the C,N,S-tridoped TiO_2 samples prepared at $R = 0$, 1, 2, 3 and 6, respectively. The indirect band-gap energy of P25 is 3.0 eV. Therefore, it is not surprising that the indirect band-gap energy

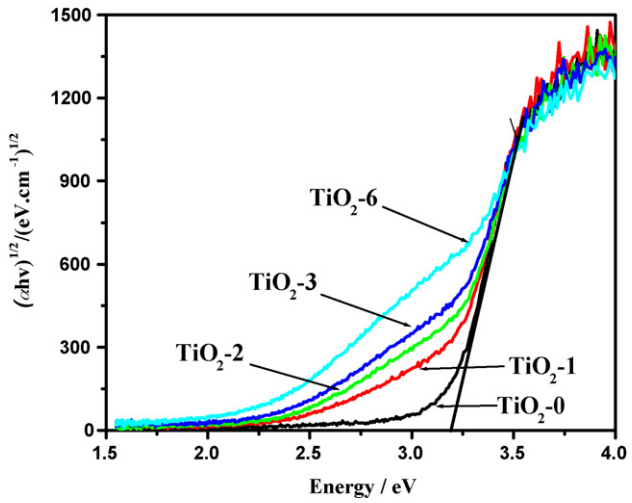

Fig. 9. Plots of the $(\alpha h\upsilon)^{1/2}$ vs. photon energy ($h\upsilon$) for the un-doped and tri-doped TiO_2 powders calcined at 500 °C.

of the as-prepared powders is much lower than that of anatase TiO_2 (pH 1, 3.2 eV) due to C,N,S-tridoping [30].

3.5. Photocatalytic activity

The photocatalytic activity of the prepared TiO_2 powders was quantificationally evaluated by the photocatalytic degradation of formaldehyde in air. However, under dark conditions without light illumination, the content of formaldehyde does not change for every measurement using various the as-prepared TiO_2 powders. Illumination in the absence of TiO_2 powders does not result in the photocatalytic reaction. Therefore, the presence of both illumination and TiO_2 powders is necessary for the efficient photocatalytic degradation. These results also suggest that the photocatalytic degradation of formaldehyde is caused by photocatalytic oxidation reactions on the surface of TiO_2 powders under the light illumination.

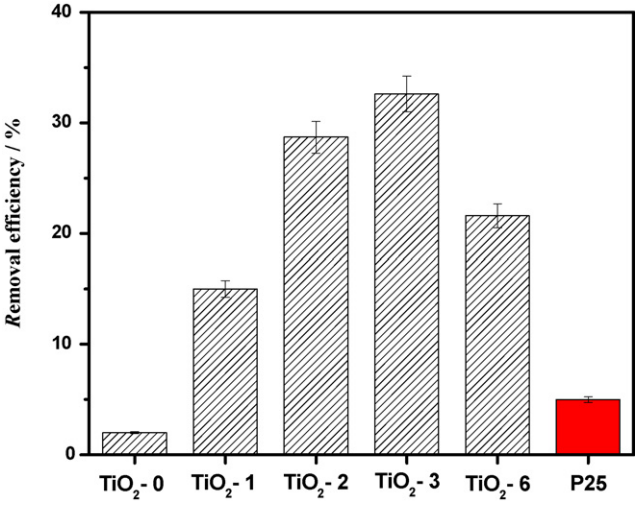

Fig. 10. The dependence of the removal efficiency (RE (%)) of photocatalytic oxidation of formaldehyde under daylight irradiation on *R*.

Fig. 10 shows the dependence of the removal efficiency (RE (%)) of photocatalytic oxidation of formaldehyde under daylight irradiation on *R*. It can be seen that the removal efficiency of the TiO_2-0 sample (without doping) has a very low-daylight-induced photocatalytic activity. This is due to the fact that the un-doped TiO_2 powders have the biggest indirect band-gap energy of about 3.2 eV. When a small amount of C, N and S atoms is doped into TiO_2 powders, the daylight-induced photocatalytic activity of the prepared samples slightly increases. At $R = 3$, the photocatalytic activity of the tri-doped sample TiO_2-3 powders reaches a maximum value, and its activity exceeds that of Degussa P25 by a factor of more than six times. With further increasing *R*, the phtotcatalytic activity of the powders decreases. The high-daylight-induced phtotcatalytic activity of the TiO_2-3 sample is due to the following factors.

Usually, the doping of C, N and S non-metal elements in TiO_2 plays an important role in its visible-light phtotcatalytic activity. It can be seen from Fig. 8 that the C,N,S-tridoping results in a intense increase in absorption in the near UV and visible-light region and a red shift in the absorption edge of the C,N,S-tridoped TiO_2 samples. This implies that the prepared tri-doped samples can be activated by visible light and more photo-generated electrons and holes can be generated and participate in the photocatalytic reactions. Hence, the band-gap narrowing of TiO_2 by C,N,S-tridoping results in enhanced photocatalytic activity of the prepared TiO_2 powders. Hashimoto and co-workers [45,46] provided an alternative explanation that a localized N 2p state formed above the valence band was the origin for the visible-light activity of the nitrogen-doped TiO_2. Yu et al. [39] found that sulfur doping can indeed create intra-band-gap states close to the conduction band edges and thus induces visible-light absorption at the sub-band-gap energy.

Apart from the above band-gap narrowing, another possible understanding is that the C,N,S-tridoped TiO_2 powder consists of two phases (un-doped and doped TiO_2). Usually, the composite of two kinds of semiconductors or two phases of the same semiconductor is beneficial in reducing the recombination of photo-generated electrons and holes and thus enhances photocatalytic activity [47–52]. The interface between the two phases may act as a rapid separation site for the photo-generated electrons and holes due to the difference in the energy level of their conduction bands and valence bands. Therefore, the C,N,S-tridoped TiO_2 powders prepared by a solid-phase reaction method exhibit a significant daylight-induced photoactivity also due to their two-phase structures (un-doped TiO_2 and C,N,S-tridoped TiO_2).

4. Conclusion

Highly photoactive mesoporous C,N,S-tridoped TiO_2 photocatalysts can be successfully prepared by a solid-phase reaction method. The C,N,S-tridoped TiO_2 powders exhibit a stronger absorption in the near UV and visible-light region and a red shift in the band-gap transition. The daylight-induced photocatalytic activities of the as-prepared C,N,S-tridoped TiO_2 powders are about six times higher than that of Degussa P25. The highly daylight-induced photoactivities of the as-prepared TiO_2 pow-

ders can be attributed to the results of the synergetic effects of strong absorption in the near UV and visible-light region, red shift in adsorption edge and two phase structures of un-doped TiO_2 and C,N,S-tridoped TiO_2.

Acknowledgements

This work was partially supported by the National Natural Science Foundation of China (20473059 and 50625208). This work was also financially supported by the Key Research Project of Chinese Ministry of Education (No. 106114), National Basic Research Program of China (2007CB613302) and Program for Changjiang Scholars and Innovative Research Team in University (PCSIRT, No. IRT0547), Ministry of Education, China.

References

[1] D. Li, H. Haneda, S. Hishita, N. Ohashi, Visible-light-driven N–F-codoped TiO_2 Photocatalysts. 1. Synthesis by spray pyrolysis and surface characterization, Chem. Mater. 17 (2005) 2588.
[2] M.A. Fox, M.T. Dulay, Heterogeneous photocatalysis, Chem. Rev. 93 (1993) 341.
[3] M.R. Hoffmann, S.T. Martin, W. Choi, D.W. Bahnemann, Environmental applications of semiconductor photocatalysis, Chem. Rev. 95 (1995) 69.
[4] H. Tada, M. Yamamoto, S. Ito, Promoting effect of MgO_x submonolayer coverage of TiO_2 on the photoinduced oxidation of anionic surfactants, Langmuir 15 (1999) 3699.
[5] A. Fujishima, T.N. Rao, D.A. Tryk, Titanium dioxide photocatalysis, J. Photochem. Photobiol. C 1 (2000) 1.
[6] K. Nagaveni, G. Sivalingam, M.S. Hegde, G. Madras, Photocatalytic degradation of organic compounds over combustion-synthesized nano-TiO_2, Environ. Sci. Technol. 38 (2004) 1600.
[7] H. Einaga, T. Ibusuki, S. Futamura, Improvement of catalyst durability by deposition of Rh on TiO_2 in photooxidation of aromatic compounds, Environ. Sci. Technol. 38 (2004) 285.
[8] P.V. Kamat, R. Huehn, R. Nicolaescu, A "Sense and Shoot" approach for photocatalytic degradation of organic contaminants in water, J. Phys. Chem. B 106 (2002) 788.
[9] F.B. Li, X.Z. Li, M.F. Hou, Photocatalytic degradation of 2-mercaptobenzothiazole in aqueous La^{3+}-TiO_2 suspension for odor control, Appl. Catal. B 48 (2004) 185.
[10] X.T. Hong, Z.P. Wang, W.M. Cai, F. Lu, J. Zhang, Y.Z. Yang, N. Ma, Y.J. Liu, Visible-light-activated nanoparticle photocatalyst of iodine-doped titanium dioxide, Chem. Mater. 17 (2005) 1548.
[11] J.C. Yu, J. Yu, W. Ho, Z. Jiang, L. Zhang, Effects of F^- doping on the photocatalytic activity and microstructures of nanocrystalline TiO_2 powders, Chem. Mater. 14 (2002) 3808.
[12] J. Soria, J.C. Conesa, V. Augugliaro, L. Palmisano, M. Schiavello, A. Sclafani, Dinitrogen photoreduction to ammonia over titanium dioxide powders doped with ferric ions, J. Phys. Chem. 95 (1991) 274.
[13] J. Premkumar, Development of super-hydrophilicity on nitrogen-doped TiO_2 thin film surface by photoelectrochemical method under visible light, Chem. Mater. 16 (2004) 3980.
[14] M. Mrowetz, W. Balcerski, A.J. Colussi, M.R. Hoffmann, Oxidative power of nitrogen-doped TiO_2 photocatalysts under visible illumination, J. Phys. Chem. B 108 (2004) 17269.
[15] D. Li, H. Haneda, S. Hishita, N. Ohashi, Visible-light-driven N–F-codoped TiO2 photocatalysts. 2. Optical characterization, photocatalysis, and potential application to air purification, Chem. Mater. 17 (2005) 2596.
[16] J.M. Mwabora, T. Lindgren, E. Avendano, T. Jaramillo, J. Lu, S.E. Lindquist, C.G. Granqvist, Structure, composition, and morphology of photoelectrochemically active $TiO_{2-x}N_x$ thin films deposited by reactive DC magnetron sputtering, J. Phys. Chem. B 108 (2004) 20193.
[17] K. Yang, Y. Dai, B. Huang, S. Han, Theoretical study of N-doped TiO_2 rutile crystals, J. Phys. Chem. B 110 (2006) 24011.
[18] H. Fu, L. Zhang, S. Zhang, Y. Zhu, J. Zhao, Electron spin resonance spin-trapping detection of radical intermediates in N-doped TiO_2-assisted photodegradation of 4-chlorophenol, J. Phys. Chem. B 110 (2006) 3061.
[19] E.A. Reyes-Garcia, Y. Sun, K. Reyes-Gil, D. Raftery, ^{15}N solid state NMR and EPR characterization of N-doped TiO_2 photocatalysts, J. Phys. Chem. C 111 (2007) 2738.
[20] J.S. Park, W. Choi, Enhanced remote photocatalytic oxidation on surface-fluorinated TiO_2, Langmuir 20 (2004) 11523.
[21] R. Asahi, T. Morikawa, T. Okwaki, K. Aoki, Y. Taga, Visible-light photocatalysis in nitrogen-doped titanium oxides, Science 293 (2001) 269.
[22] T. Umebayashi, T. Yamaki, H. Itoh, K. Asai, Band-gap narrowing of titanium dioxide by sulfur doping, Appl. Phys. Lett. 81 (2002) 454.
[23] T. Umebayashi, T. Yamaki, S. Tanala, K. Asai, Visible light-induced degradation of methylene blue on S-doped TiO_2, Chem. Lett. 32 (2003) 330.
[24] T. Umebayashi, T. Yamaki, S. Yamamoto, A. Miyashita, S. Tanala, T. Sumita, K. Asai, Sulfur-doping of rutile-titanium dioxide by ion implantation: photocurrent spectroscopy and first-principles band calculation studies, J. Appl. Phys. 93 (2003) 5156.
[25] T. Ohno, T. Mitsui, M. Matsumura, Photocatalytic activity of S-doped TiO_2 photocatalyst under visible light, Chem. Lett. 32 (2003) 364.
[26] T. Ohno, M. Akiyoshi, T. Umebayashi, K. Asai, T. Mitsui, M. Matsumura, Preparation of S-doped TiO_2 photocatalysts and their photocatalytic activities under visible light, Appl. Catal. A 265 (2004) 115.
[27] T. Ohno, Preparation of visible light active S-doped TiO_2 photocatalysts and their photocatalytic activities, Water Sci. Technol. 49 (2004) 159.
[28] W. Zhao, W. Ma, C. Chen, J. Zhao, Z. Shuai, Efficient degradation of toxic organic pollutants with $Ni_2O_3/TiO_{2-x}B_x$ under visible irradiation, J. Am. Chem. Soc. 126 (2004) 4782.
[29] T. Tachikawa, S. Tojo, K. Kawai, M. Endo, M. Fujitsuka, T. Ohno, K. Nishijima, Z. Miyamoto, T. Majima, Photocatalytic oxidation reactivity of holes in the sulfur- and carbon-doped TiO_2 powders studied by time-resolved diffuse reflectance spectroscopy, J. Phys. Chem. B 108 (2004) 19299.
[30] J. Yu, M. Zhou, B. Cheng, X. Zhao, Preparation, characterization and photocatalytic of in situ N,S-codoped TiO_2 powders, J. Mol. Catal. A 246 (2006) 176.
[31] K.S.W. Sing, D.H. Everett, R.A.W. Haul, L. Moscou, R.A. Pierotti, J. Rouquerol, T. Siemieniewska, Reporting physisorption data for gas/solid systems with special reference to the determination of surface area and porosity, Pure Appl. Chem. 57 (1985) 603.
[32] J. Yu, M. Zhou, B. Cheng, H. Yu, X. Zhao, Ultrasonic preparation of mesoporous titanium dioxide nanocrystalline photocatalysts and evaluation of photocatalytic activity, J. Mol. Catal. A 227 (2005) 75.
[33] M. Zhou, J. Yu, B. Cheng, H.G. Yu, Preparation and photocatalytic activity of Fe-doped mesoporous titanium dioxide nanocrystalline photocatalysts, Mater. Chem. Phys. 93 (2005) 159.
[34] B. Lindberg, R. Maripuu, K. Siegbahn, R. Larsson, C.G. Golander, J.C. Eriksson, ESCA studies of heparinized and related surfaces. I. Model surfaces on steel substrates, J. Colloid Interface Sci. 95 (1983) 308.
[35] J. Yu, Y. Su, B. Cheng, M. Zhou, Effects of pH on the microstructures and photocatalytic activity of mesoporous nanocrystalline titania powders prepared via hydrothermal method, J. Mol. Catal. A 258 (2006) 104.
[36] O. Diwald, T.L. Thompson, E. Zubkov, E.G. Goralski, S.D. Walck, J.T. Yates Jr., Photochemical activity of nitrogen-doped rutile TiO_2(1 1 0) in visible light, J. Phys. Chem. B 108 (2004) 6004.
[37] R. Nakamura, T. Tanaka, Y. Nakato, Mechanism for visible light responses in anodic photocurrents at N-doped TiO_2 film electrodes, J. Phys. Chem. B 108 (2004) 10617.
[38] S. Sakthivel, M. Janczarek, H. Kisch, Visible light activity and photoelectrochemical properties of nitrogen-doped TiO_2, J. Phys. Chem. B 108 (2004) 19384.
[39] J.C. Yu, W.K. Ho, J.G. Yu, H. Yip, P.K. Wong, J.C. Zhao, Efficient visible-light-induced photocatalytic disinfection on sulfur-doped nanocrystalline titania, Environ. Sci. Technol. 39 (2005) 1175.
[40] R. Bacsa, J. Kiwi, T. Ohno, P. Albers, V. Nadtochenko, Preparation, testing and characterization of doped TiO_2 active in the peroxidation of biomolecules under visible light, J. Phys. Chem. B 109 (2005) 5994.

[41] W. Huang, X. Tang, Y. Wang, Y. Koltypin, A. Gedanken, Selective synthesis of anatase and rutile *via* ultrasound irradiation, Chem. Commun. 15 (2000) 1415.

[42] N. Serpone, D. Lawless, R. Khairutdinov, Size effects on the photophysical properties of colloidal anatase TiO_2 particles: size quantization or direct transitions in this indirect semiconductor? J. Phys. Chem. 99 (1995) 16646.

[43] X.H. Wang, J.G. Li, H. Kamiyama, M. Katada, N. Ohashi, Y. Moriyoshi, T. Ishigaki, Pyrogenic iron(III)-doped TiO_2 nanopowders synthesized in RF thermal plasma: phase formation, defect structure, band gap, and magnetic properties, J. Am. Chem. Soc. 127 (2005) 10982.

[44] H. Yu, J. Yu, B. Cheng, M. Zhou, Effects of hydrothermal post-treatment on microstructures and morphology of titanate nanoribbons, J. Solid State Chem. 179 (2006) 349.

[45] H. Irie, S. Washizuka, N. Yoshino, K. Hashimoto, Visible-light induced hydrophilicity on nitrogen-substituted titanium dioxide films, Chem. Commun. (2003) 1298.

[46] H. Irie, Y. Watanabe, K. Hashimoto, Nitrogen-concentration dependence on photocatalytic activity of $TiO_{2-x}N_x$ powders, J. Phys. Chem. B 107 (2003) 5483.

[47] J. Yu, H. Yu, B. Cheng, X. Zhao, J.C. Yu, W. Ho, The effect of calcination temperature on the surface microstructure and photocatalytic activity of TiO2 thin films prepared by liquid phase deposition, J. Phys. Chem. B 107 (2003) 13871.

[48] J. Yu, J.C. Yu, M.K.P. Leung, W. Ho, B. Cheng, X. Zhao, J. Zhao, Effects of acidic and basic hydrolysis catalysts on the photocatalytic activity and microstructures of bimodal mesoporous titania, J. Catal. 217 (2003) 69.

[49] M. Zhou, J. Yu, B. Cheng, Effects of Fe-doping on the photocatalytic activity of mesoporous TiO_2 powders prepared by an ultrasonic method, J. Hazard. Mater. 137 (2006) 1838.

[50] J. Yu, J. Xiong, B. Cheng, S. Liu, Fabrication and characterization of Ag-TiO2 multiphase nanocomposite thin films with enhanced photocatalytic activity, Appl. Catal. B 60 (2005) 211.

[51] J. Yu, L. Zhang, B. Cheng, Y. Su, Hydrothermal preparation and photocatalytic activity of hierarchically sponge-like macro/mesoporous titania, J. Phys. Chem. C 111 (2007) 10582.

[52] J. Yu, S. Liu, H. Yu, Microstructures and photoactivity of mesoporous anatase hollow microspheres fabricated by fluoride-mediated self-transformation, J. Catal. 249 (2007) 59.